Dalton Transactions

Accepted Manuscript

ROYAL SOCIETY OF CHEMISTRY

www.rsc.org/dalton

Journal Name

RSCPublishing

COMMUNICATION

Complete Surface Coverage of ZnO Nanorod Arrays by Pulsed electrodeposited $CuInS_2$ for Visible Light Energy Conversion

Cite this: DOI: 10.1039/x0xx00000x

Received 00th January 2012,
Accepted 00th January 2012

DOI: 10.1039/x0xx00000x

www.rsc.org/

Yiming Tang,[a] Jung-Ho Yun,[b] Lianzhou Wang,[b] Rose Amal[a*] and Yun Hau Ng[a*]

Well-aligned ZnO nanorods were uniformly coated with a layer of $CuInS_2$ nanoparticle photosensitizers using a tailored sequential pulsed-electrodeposition. The formation of $CuInS_2$-ZnO heterojunction with well-matched band energy alignment and the superior electron mobility in ZnO nanorods led to remarkable 3.75 times improved photoelectrochemical performance of the electrode under visible light irradiation.

Owing to the distinct electron transport behaviour, one dimensional (1D) nanoarray of photoactive oxide materials has attracted much attention in the design of photovoltaics, liquid state photoelectrochemical cells, and photocatalysis.[1] Semiconducting TiO_2, Fe_2O_3, WO_3 and ZnO, for examples, have been designed in the fashions of nanotubes, nanorods, nanowires, nanoneedles and many other 1D-nanostructures.[2] They could be in either highly ordered or randomly packed manner.[3] To extend the light-response of these wide band gap 1D-nanostructured oxides, decoration with narrow bandgap materials as photosensitizers is a popular and effective strategy.[4] Although powder of these oxides can be conveniently coated with binary and ternary photosensitizers (e.g. CdS and $CuInS_2$) using hydro(solvo-)thermal method,[5] it remains a great challenge to directly cover the surface of the 1D-nanostructures in the thin film configuration. For thin films, electrodeposition is a simple and effective technique to decorate compact films with a wide range of metallic components, but due to the differences in the deposition kinetics and mechanisms, coating the arrays of well-aligned nanorods and nanotubes thin films with secondary components always results in inadequate coverage of the 1D-nanostructures and it is mostly limited to the top layer (or entrance) of the 1D-nanostructures. A generally accepted reason is that a gradient of precursor concentration exists throughout the length of the 1D-nanostructures. Higher concentration of the precursor at the top region of the 1D-nanostructures induces rapid nucleation or deposition when cathodic bias is applied. This leads to the immediate formation of the secondary component at the top region (entrance) and subsequently blocks/slows the diffusion of fresh precursor into the deeper region for successive deposition.

$CuInS_2$ is a visible light active semiconductor with a chalcogenide-type crystal structure. It demonstrates great potential in photovoltaic and solar hydrogen applications.[6] Unlike depositing binary sulphides, electrodeposition of the ternary sulphide $CuInS_2$ is more challenging as it involves multi elemental deposition. The objective of this work is, therefore, to uniformly deposit $CuInS_2$ nanoparticles on vertically aligned ZnO nanorod arrays grown on a transparent charge collecting electrode, i.e. fluorine-doped tin oxide (FTO) glass substrate. The creation of effective junctions between ZnO and $CuInS_2$ will allow superior charge transfer from the photoexcited $CuInS_2$ to ZnO upon illumination. The charges can be efficiently collected at the charge collecting electrode to improve the charges utilisation. Together with greater light penetration into deeper region of the 1-D nanostructured film, the pulsed-electrodeposited $CuInS_2$ thin film is expected to show improved photoelectrochemical activities. ZnO nanorod is chosen as it possesses extreme high electron mobility (200-300 cm^2Vs^{-1}), a value greater than that of the benchmark semiconductor TiO_2 (0.1-4 cm^2Vs^{-1}). Coating of ZnO with $CuInS_2$ offers vast opportunities in further improving the photoresponse of light-active semiconductor.[7] Depositing this multi-component $CuInS_2$ on ZnO is, however, challenged by the stability of ZnO in the precursor media with varied pH. Precursor of indium (typically $InCl_3$) has a pH value of 3-4 which imposes gradual dissolution of ZnO during the electrodeposition.[8] A new strategy tailored for ZnO coating with multi-element (not limited to $CuInS_2$) is therefore in high demand in the area of photoelectrochemical studies.

In this communication, we present a square wave sequential pulsed-electrodeposition approach to wrap the ZnO nanorods with $CuInS_2$ nanoparticles. The well-aligned ZnO nanorod arrays were prepared using an established method of chemical bath deposition (CBD).[9] Detailed experimental conditions are included in the *Supplementary Information* (Table S1). X-ray diffraction (XRD) pattern in Figure 1a shows the successful formation of crystallized ZnO with the dominant (002) plane on the fluorine-doped tin oxide (FTO) glass substrate. Based on these ZnO nanorods, $CuInS_2$ nanoparticles were pulsed-electrodeposited at the frequency of 5 Hz using three different pulsing conditions: (1) Cu deposition followed by In; (2) In deposition followed by Cu; and (3) simultaneous Cu and In deposition. $Na_2S_2O_3$ is always present in the initial pulsed electrodeposition to ensure the incorporation of sulphur component

for the subsequent formation of $CuInS_2$ nanocrystals. Figure 1b-1d shows the XRD patterns of the resultant $CuInS_2$-ZnO thin films with the above mentioned conditions. All XRD patterns prove the presence of $CuInS_2$ with the main (112) peak at 27.4°.

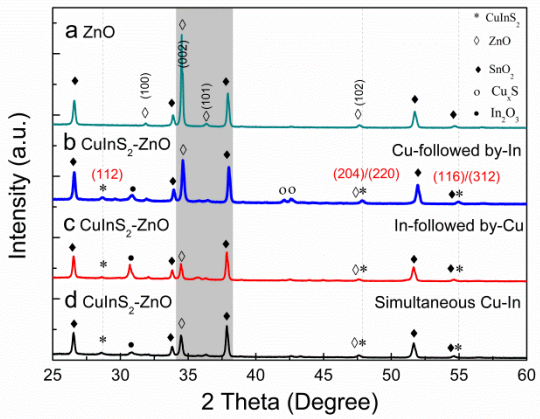

Figure 1 XRD patterns of the (a) ZnO film and (b-d) $CuInS_2$-ZnO films with various deposition conditions.

Noticeably, the peak intensity of ZnO (002) plane relative to the FTO peak was significantly decreased when the $CuInS_2$-ZnO were prepared using the In-deposition followed by Cu sequence (Figure 1c) and simultaneous Cu-In deposition (Figure 1d). The inductively coupled plasma-atomic emission spectroscopy (ICP-AES) analyses of the post-deposition electrolytes indicate the substantial amount of dissolved Zn in the latter two samples (11.6 ppm for the simultaneous Cu-In deposition; 11 ppm for the In-followed by-Cu deposition) while the Cu-followed by-In deposition sample shows only mild dissolution of ZnO (0.13 ppm of dissolved Zn). The severity of the ZnO dissolution during the $CuInS_2$ pulsed-electrodeposition was subsequently identified to be related to the pH of the initial precursor solutions. pH 3.8 and pH 3.9 were measured, respectively, for the precursor solutions of the simultaneous Cu-In deposition and the In-followed by-Cu deposition. The suppression of the ZnO dissolution in the Cu-followed by-In deposition system was attributed to the ability of thiosulfate ions from $Na_2S_2O_3$ to reduce the Cu (II) ion and instantaneously complexing with the resulting Cu (I) species. The formation of this stable complex can suppress the release of H^+ from the Cu ions hydrolysis.[10] Therefore, a higher pH value of 6.8 observed in this system resulted in the less substantial ZnO dissolution. No similar complex had been reported for the In ions. Cu-followed by-In deposited $CuInS_2$-ZnO was, therefore, chosen as the optimized thin film for further investigation.

Figure 2 shows the scanning (SEM) and transmission electron microscopy (TEM) images of ZnO and $CuInS_2$-ZnO derived from the Cu-followed by-In deposition sequence. Vertically aligned ZnO nanorods with average diameter of ca. 70 nm were grown on the FTO substrate. The TEM images (Figure 2b and c) with well-defined lattice fringe of 0.26 nm ((001) plane) show highly crystalline ZnO nanorods with the relatively smooth surface, indicating the undecorated morphology of ZnO. Introducing regulated pulsed condition (5 Hz) in the electrodeposition successfully wrapped the ZnO nanorods evenly with $CuInS_2$ nanoparticles. Slightly thicker and rougher surface of the nanorods (Figure 2e) indicate the deposition of nanoparticles on the ZnO, in which the nanoparticles were identified to be the crystalline $CuInS_2$ (Figure 2f). Note that this uniformly coated ZnO nanorods thin film was rarely seen in the samples prepared with conventional non-pulsed electrodeposition method.[11] As shown in Figure S1 (*Supplementary Information*), non-pulsed electrodeposition led to the formation of thick $CuInS_2$ layer only on top of the ZnO nanorod arrays. Thus, the presence of pulse at appropriate frequency during the electrodeposition is critical in ensuring the uniform photosensitizer coating on individual nanorods.

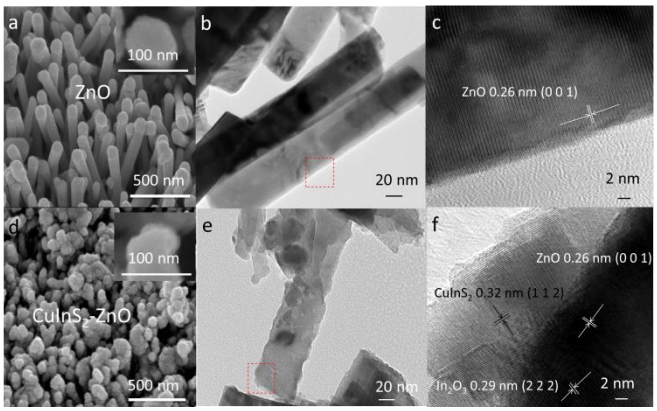

Figure 2 (a-c) show the surface morphology of ZnO nanorods (+30° tiled view), TEM image of an individual ZnO nanorod and HRTEM image of the ZnO nanorod, respectively; (d-f) show the surface morphology of $CuInS_2$-ZnO film (+30° tiled view), TEM image of an individual $CuInS_2$-ZnO nanorod and HRTEM image of the $CuInS_2$-ZnO nanorod.

It is of interest to discuss the effect of electrodeposition condition on the formation of $CuInS_2$ coating. The square wave pulse in this work was set at a cathodic bias (-1.25V, 100 ms) and a relaxation bias (0V, 100 ms), respectively. The nucleation of Cu and In was induced at cathodic bias to form Cu/In/S intermediate (before the calcination) while the relaxation bias provided sufficient diffusion time for the fresh precursor to reach the un-nucleated sites of ZnO. The repetition of this nucleation-diffusion cycles eventually results in the wrapping of ZnO nanorods with $CuInS_2$ nanoparticles. In contrast, the non-pulsing condition introduces continuing nucleation energy for the deposition of $CuInS_2$ throughout the deposition. The initial $CuInS_2$ nanoparticles formed on the tip of the ZnO nanorods rapidly grow into a bulky and fused $CuInS_2$ layer which causes the ultimate blockage of the entrance to the deeper sites of ZnO nanorods. As a result, an ineffective coverage and poor heterojunction of $CuInS_2$-ZnO was formed from the non-pulsed electrodeposition.

Figure 3a shows the Tauc plots of ZnO and $CuInS_2$-ZnO nanorod arrays. While bare ZnO nanorods demonstrate the typical optical bandgap of 3.25 eV, $CuInS_2$-ZnO has extended its photoresponse to visible light region. Optical band gap of 1.3 eV was measured on the bare $CuInS_2$ thin film prepared using this method and it is in good agreement with reported values.[6] The considerable absorbance in the window of 390 - 920 nm reveals the origin of the visible light photocurrent generation, which will be discussed later. In addition to the extended light absorption, electrochemical impedance spectra (EIS) (Figure 3b) of bare ZnO nanorods, bare $CuInS_2$ film and $CuInS_2$-ZnO film performed under visible light illumination provide useful insight on the bulk conductance of the films. At high frequency (>500 Hz), the conductance of each film is dominated by the electrolyte used in the measurement and therefore similar value was obtained. The film conductance was indicated in the frequency ranged from 10 mHz to 500 Hz.[12] The visible light-excited $CuInS_2$-ZnO thin film exhibited the highest conductance compared with the individual component of ZnO film and $CuInS_2$ film. Under visible

light, bare ZnO film was not excited thus the intrinsic conductance of the ZnO was shown. Although the bare $CuInS_2$ film was excited, its limited charge diffusion resulted in moderate bulk conductance. When combined, $CuInS_2$-ZnO film demonstrated superior film conductance as the excited charges from $CuInS_2$ were transferred to ZnO. Owing to the better electron mobility in ZnO, the film conductance is therefore enhanced in the illuminated $CuInS_2$-ZnO.

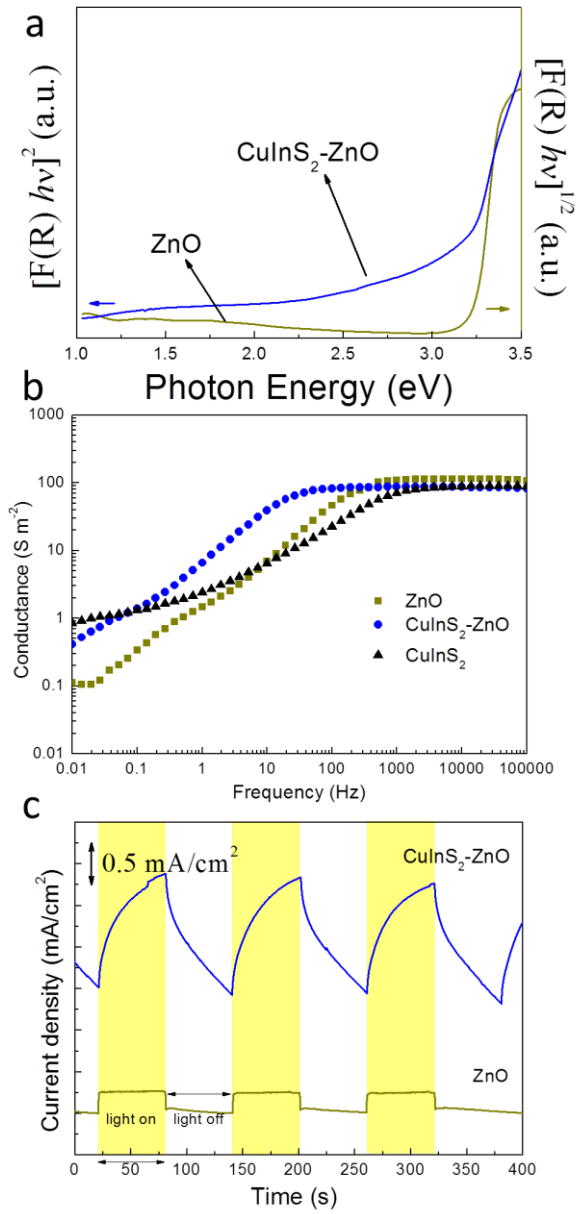

Figure 3 (a) Tauc plots of ZnO and $CuInS_2$-ZnO arrays prepared by "Cu-followed by-In" sequence; (b) EIS conductance plots of ZnO and $CuInS_2$-ZnO film prepared by "Cu-followed by-In" sequence in 0.1 mol/L lithium perchlorate ($LiClO_4$) in acetonitrile (CH_3CN) solution under visible light illumination; (c) Photocurrent response of ZnO and $CuInS_2$-ZnO film prepared by "Cu-followed by-In" method at 0.75 V vs Ag/AgCl in an electrolyte containing 0.25 mol/L Na_2S and 0.35 mol/L Na_2SO_3 (pH = 12) under visible light irradiation ($\lambda \geq 435$ nm).

The constructive effects of extended light absorption and improved film conductance in $CuInS_2$-ZnO nanorods were reflected in their photoelectrochemical current generation. Figure 3c shows the amperometric photoresponses of ZnO and $CuInS_2$-ZnO nanorod arrays under visible light illumination. $CuInS_2$ is determined to be n-type semiconductor as it demonstrated anodic photocurrent upon visible light illumination (Figure S2). Under illumination with $\lambda >$ 435 nm, $CuInS_2$ component in the composite undergoes charge separation to excite electrons to its conduction band. The difference energy level between the conduction bands of $CuInS_2$ and ZnO introduces an internal local electric field at the heterojunction that drives the electron transfer from $CuInS_2$ to ZnO.[13] As ZnO has great electron mobility, the injected electrons are efficiently transported to the external circuit to generate photocurrent. The $CuInS_2$-ZnO nanorod arrays prepared by the Cu-followed by-In deposition sequence show the highest photocurrent density of 1.5 mA/cm^2. The photocurrent generation during the on-off illumination cycles was reproducible although the photoresponses were relatively slow (as indicated by the gradual increase of the current upon illumination) compared with oxide-based photoactive films due to its slower electron transfer kinetics.[14] For comparison, $CuInS_2$-ZnO nanorod arrays derived from the simultaneous Cu-In deposition and In-followed by-Cu deposition sequence only generated 0.6 and 0.4 mA/cm^2, respectively (see Figure S3 in *Supplementary Information*). The lower photocurrent generated in these two samples are attributed to two reasons: (i) severe dissolution of ZnO component during $CuInS_2$ deposition as evident by lower XRD peak for ZnO together with the dissolved ZnO measured by ICP, and (ii) the formation of impurities such as the interface In_2O_3 revealed by HRTEM. These results highlight the importance of tailoring the deposition condition according to the specific properties of the host materials (ZnO nanorods in this work and TiO_2 nanotubes in our previous report[4]). Photocurrent density of 0.25 mA/cm^2 was observed in the bare ZnO nanorods and the excitation is attributed to the remnant UV component of the incident light that passed through the optical cut-off filter. [15]

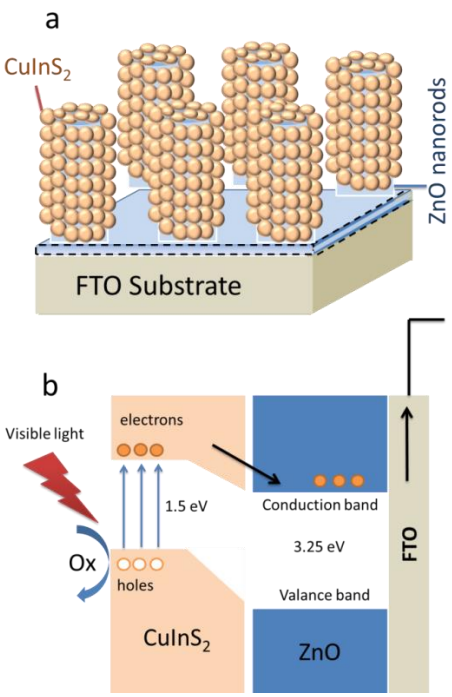

Figure 4 (a) Schematic diagram of the $CuInS_2$-ZnO film; (b) Electronic structures of $CuInS_2$-ZnO film.

Schematic illustration of $CuInS_2$-ZnO structure (Figure 4a) depicts the close vicinity and effective contact between $CuInS_2$ nanoparticles and ZnO nanorods derived from the sequential pulsed-electrodeposition. The well-matched band alignment of these two components as shown in Figure 4b also promotes the transfer of excited electrons from $CuInS_2$. Lastly, the superior electron mobility in ZnO allows the efficient transportation of the injected charge to be utilized at the counter electrode.

In summary, tailored deposition sequence was found influential in fabricating $CuInS_2$-ZnO nanorods with effective heterojunction. Square wave pulsed condition was the key to lead to a complete coating of the ZnO nanorods with an even layer of $CuInS_2$ nanoparticles. A high quality heterojunction further empowered by the energetically favoured band alignment facilitated good photoelectrochemical performances.

Acknowledgements

This work has been supported by the Australian Research Council Discovery Project (DP110101638). Yiming Tang also acknowledges the scholarship under the State Scholarship Fund awarded by China Scholarship Council. The authors would also like to acknowledge the UNSW Mark Wainwright Analytical Centre, and particularly thank Dr. Katie Levick for her generous help in the TEM analysis.

Notes and references

[a] Particles and Catalysis Research Group, School of Chemical Engineering, The University of New South Wales, Sydney NSW 2052, Australia.

[b] Nanomaterials Centre, School of Chemical Engineering and AIBN, The University of Queensland, QLD 4072, Australia.

† Electronic Supplementary Information (ESI) available: [Experimental details; SEM image of $CuInS_2$-ZnO from non-pulsed electrodeposition and additional PEC measurement of pulsed electrodeposited $CuInS_2$-ZnO under different conditions are involved]. See DOI: 10.1039/c000000x/

1 (a) K. Kiatkittipong, J. Scott and R. Amal, *ACS Appl. Mater. Interfaces*, 2011, **3**, 3988; (b) C.M. Johnson, P.J. Reece and G.J. Conibeer, *Opt. Lett.*, 2011, **36**, 3990; (c) J. Xiong, Z. Li, J. Chen, S. Zhang, L. Wang and S. Dou, *ACS Appl. Mater. Interface*, 2014, **6**, 15716.

2 (a) Y. Bai, H. Yu, Z. Li, R. Amal, G.Q. Lu and L. Wang, *Adv. Mater.*, 2012, **24**, 5850; (b) J.-H. Yun, Y.H. Ng, C. Ye, A.J. Mozer, G.G. Wallace and R. Amal, *ACS Appl. Mater. Interface*, 2011, **3**, 1585; (c) Y. Ling, G. Wang, D.A. Wheeler, J.Z. Zhang and Y. Li, *Nano Lett.*, 2011, **11**, 2119; (d) C. Ng, C. Ye, Y.H. Ng and R. Amal, *Cryst. Growth Des.*, 2010, **10**, 3794; (e) M. Law, L.E. Greene, J.C. Johnson, R. Saykally and P. Yang, *Nat. Mater.*, 2005, **4**, 455.

3 S. Xu and Z. Wang, *Nano Res.*, 2011, **4**, 1013.

4 J.-H. Yun, Y.H. Ng, S. Huang, G. Conibeer and R. Amal, *Chem. Commun.*, 2011, **47**, 11288.

5 (a) F. Shen, W. Que, Y. He, Y. Yuan, X. Yin and G. Wang, *ACS Appl. Mater. Interfaces*, 2012, **4**, 4087; (b) Y. Li, Z. Liu, Y. Wang, Z. Liu, J. Han and J. Ya, *Int. J. Hydrogen Energy*, 2012, **37**, 15029.

6 (a) Y. Tang, Y.H. Ng, J.-H. Yun and R. Amal, *RSC Adv.*, 2014, **4**, 3278.; (b) F. M. Courtel, A. Hammami, R. Imbeault, G. Hersant, R. W. Paynter, B. Marsan, M. Morin, *Chem. Mater.*, 2010, **22**, 3752.

7 U. Özgür, Y.I. Alivov, C. Liu, A. Teke, M.A. Reshchikov, S. Doğan, V. Avrutin, S.J. Cho and H. Morkoç, *J. Appl. Phys.*, 2005, **98**, 041301.

8 (a) S. Sanchez, D. Aldakov, D. Rouchon, L. Rapenne, A. Delamoreanu, C. Levy-Clement and V. Ivanova, *J. Renewable Sustainable Energy*, 2013, **5**, 011207; (b) S. Peulon and D. Lincot, *J. Electrochem Soc.*, 1998, **145**, 864.

9 L. Vayssieres, K. Keis, S.–E. Lindquist and A. Hagfeldt, *J. Phys. Chem. B*, 2001, **105**, 3350.

10 T. Yukawa, K. Kuwabara and K. Koumoto, *Thin Solid Films*, 1996, **280**, 160.

11 S. Sanchez, D. Aldakov, D. Rouchon, L. Rapenne, A. Delamoreanu, C. Levy-Clement and V. Ivanova, *J. Renewable Sustainable Energy*, 2013, **5**, 011207

12 N.J. Bell, Y.H. Ng, A. Du, H. Coster, S.C. Smith and R. Amal, *J. Phys. Chem. C*, 2011, **115**, 6004.

13 (a) T.L. Li, Y.L. Lee and H.S. Teng, *J. Mater. Chem.*, 2011, **21**, 5089; (b) R. Loef, J. Schoonman and A. Goossens, *J. Appl. Phys.*, 2007, **102**, 024512.

14 Y.H. Ng, A. Iwase, N. J. Bell, A. Kudo and R. Amal, *Catal. Today*, 2011, **164**, 353.

15 Y. Choi, M. Beak and K. Yong, *Nanoscale*, 2014, **6**, 8914

